Preparation and thermoelectric properties of BaMn2−xZnxSb2 zintl compounds

ARTICLE *in* JOURNAL OF MATERIALS SCIENCE MATERIALS IN ELECTRONICS · DECEMBER 2012

Impact Factor: 1.57 · DOI: 10.1007/s10854-012-0820-8

J Mater Sci: Mater Electron (2012) 23:2289–2292
DOI 10.1007/s10854-012-0820-8

Preparation and thermoelectric properties of $BaMn_{2-x}Zn_xSb_2$ zintl compounds

H. F. Wang · K. F. Cai · S. Chen

Received: 7 April 2012 / Accepted: 27 June 2012 / Published online: 6 July 2012

Abstract Zn doped $BaMn_2Sb_2$ single crystals were synthesized by a Sn-flux method using nominal compositions of $BaMn_{2-x}Zn_xSb_2$ (x = 0.0, 0.3, 0.5, 0.7, and 1.0). The products were characterized by powder X-ray diffraction and scanning electron microscopy equipped with electron energy dispersive spectroscopy, respectively. A pure phase of $BaMn_2Sb_2$ for x = 0, a mixture of Zn doped $BaMn_2Sb_2$ and Sn for x = 0.3–0.7, and a mixture of Zn doped $BaMn_2Sb_2$, Sn and ZnSb for x = 1 were obtained. The electrical conductivity and Seebeck coefficient of the crystals from room temperature to 773 K were measured. The electrical conductivity of all the crystals increased with increasing temperature, while the Seebeck coefficient decreased with increasing temperature and approached negative values at high temperatures. The Zn doped $BaMn_2Sb_2$ crystals showed significantly higher Seebeck coefficient at low temperatures (T < 550 K) and lower electrical conductivity at higher temperatures (T > 550 K) than the $BaMn_2Sb_2$ single crystal.

1 Introduction

Recently, high performance thermoelectric (TE) materials for applications in power generation and cooling have attracted great attention [1]. The efficiency of a TE material is determined by the dimensionless figure of merit $ZT = (\alpha^2\sigma/\kappa)T$, where α is the Seebeck coefficient, σ the electrical conductivity, κ the total thermal conductivity, and T the absolute temperature. It is known from this equation that a good TE material should require a combination of large Seebeck coefficient, high electrical conductivity and low thermal conductivity [2].

Zintl compounds are, in general, electronically positioned between intermetallics and insulating valence compounds. They are typically characterized by a small semiconducting gap and charge counting arguments can be used as a mechanism to stabilize certain crystal structures [3]. Since 2006, when Kauzlarich and coworkers [4] reported that $Yb_{14}MnSb_{11}$ Zintl compound has unexpected and exceptional TE properties (ZT ~ 1 at 1223 K), more and more attentions have been paid to Zintl compounds [5–17], and significant progress has been made. For example, Kauzlarich and coworkers further improved the TE properties of the $Yb_{14}MnSb_{11}$ Zintl compound by doping La at Yb site (ZT = 1.15 at 1100 K for $Yb_{13.6}La_{0.4}MnSb_{11}$) [9], Zn at Mn site (ZT = 1.1 at 1275 K for $Yb_{14}Mn_{0.6}Zn_{0.4}Sb_{11}$) [10], and Al at Mn site (ZT = 1.3 at 1223 K for $Yb_{14}Mn_{1-x}Al_xSb_{11}$, x = 0.6 and 0.8) [11]. Zhao et al. found that 1-2-2 type Zintl compounds also have high ZT values: ZT = 0.92 for $EuZn_2Sb_2$ at 750 K [14], and ZT = 1.2 at 700 K for $YbCd_{1.6}Zn_{0.4}Sb_2$ [15].

As a ternary Zintl compound, $BaMn_2Sb_2$ possesses a body-centered tetragonal $ThCr_2Si_2$ crystal structure (space group, I4/mmm). In the structure, planes of Ba–Sb–Mn–Sb–Ba–… stack along the c-axis and the Mn atom has a tetrahedral coordination with respect to the Sb atom. Brechtel et al. [18] synthesized $BaMn_2Sb_2$ crystals by a stoichiometric synthesis method. Xia et al. [19] grew $BaMn_2Sb_2$ crystals using Sn as metal flux and studied the electronic structure and magnetic properties of the crystals using the linear muffin-tin orbital method. An et al. [20] calculated the electronic and magnetic properties of $BaMn_2Sb_2$ using density functional calculations. The crystals grown by a Sn-flux method are usually bigger than

H. F. Wang · K. F. Cai (✉) · S. Chen
Functional Materials Research Laboratory, Tongji University, 1239 Siping Road, Shanghai 200092, China
e-mail: kfcai@tongji.edu.cn

those prepared by a stoichiometric synthesis method. We [21] recently synthesized $BaMn_2Sb_2$ single crystals by a Sn-flux method and studied the TE properties of the $BaMn_2Sb_2$ single crystals. In this work, Zn doped $BaMn_2Sb_2$ crystals were also grown by the Sn-flux method, and the TE properties of the crystals were measured from room temperature to 723 K.

2 Experimental details

Ba pieces (Alfa Aesar, 99.2 %), Mn flakes (Johnson Matthey, 99.9 %), Zn powder (Sinopharm Chemical Reagent, 99.999 %), Sb powder (Sinopharm Chemical Reagent, 99.99 %) and Sn powder (Sinopharm Chemical Reagent, 99.5 %) were used as the starting materials. All manipulations were performed in an argon-filled glove box. The mixture of all elements of Ba, Mn, Zn, Sb, Sn in the molar ratios of 1:2 − x:x:2:14 (x = 0, 0.3, 0.5, 0.7, 1) was placed in a 5-cm^3 corundum crucible. The reactants were sealed in quartz ampoules under 1/5 atm argon atmosphere and placed in a high-temperature programmable furnace. The reactants were heated to 1373 K with a rate of 600 K/h, then held at 1373 K for 1 h, followed by slowly cooling (−2 K/h) down to 1023 K. Upon reaching 1023 K, the ampoules were inverted and spun in a centrifuge at 4000 rpm for 5 min to separate the products from the Sn flux. High yield of reflective and silver-colored sheet-like single crystals were obtained. The crystals are moderately sensitive to air, as evidenced from the gradually loss of their luster when exposed to air for a few hours.

Several small crystals were ground into powder for X-ray diffraction (XRD, Rigaku, D/max2550) analysis to investigate the phase composition. The fracture surface of the crystals was observed by scanning electron microscopy (SEM, JEOL JSM5510LV), equipped with electron energy dispersive X-ray spectroscopy (EDS, Oxford 7582). Hall effect measurement was carried out at room temperature using a Hall effect measurement system (HMS 3000, Ecopia) with a magnetic field of 0.55 T. Big crystals were cut into small rectangles ($\sim 1 \times 1 \times 5$ mm^3) for TE properties measurement. The σ and α measurements were carried out using a home-made computer control test system from room temperature to 723 K under argon atmosphere. The σ measurement was performed by a steady-state four-probe technique with a square wave current ($\sim$10 mA in amplitude). The α value was determined by the slope of the linear relationship between the thermal electromotive force and temperature difference ($\sim$10 K) between the two ends of each sample. Thermal electromotive force was measured by using two K-type NiCr–NiSi thermocouples attached to the two ends of each sample. The error of the measured Seebeck coefficient values is less than 10 %.

3 Results and discussion

Figure 1(a) shows powder XRD patterns for the crystals synthesized, and the pattern of the reported $BaMn_2Sb_2$ (JCPDS card 33-0094) is also shown for comparison. The XRD analysis indicates that the sample $BaMn_{2-x}Zn_xSb_2$ (x = 0) is a pure $BaMn_2Sb_2$ without any impurity phase. The samples of $BaMn_{2-x}Zn_xSb_2$ (x = 0.3–0.7) contain both $BaMn_2Sb_2$ and Sn, while the sample of $BaMn_{2-x}Zn_xSb_2$ (x = 1) consists of $BaMn_2Sb_2$, hexagonal ZnSb and Sn. In the samples of $BaMn_{2-x}Zn_xSb_2$ (x = 0.3–0.7), no Zn-contained impurity phase was detected, indicating that Zn was successfully doped into the $BaMn_2Sb_2$. The Sn impurity phase is believed to originate from the Sn-flux contamination at the surface of the crystals. The appearance of the ZnSb phase for the sample of the $BaMn_{2-x}Zn_xSb_2$ (x = 1) suggests that the maximum Zn doping concentration, x, in $BaMn_2Sb_2$ can not exceed 1 under the present synthesis condition. Due to the ZnSb impurity phase, further TE studies on the sample of $BaMn_{2-x}Zn_xSb_2$ (x = 1) were not carried out.

SEM observation reveals that like the $BaMn_2Sb_2$ reported in Ref. [21], the $BaMn_{2-x}Zn_xSb_2$ (x = 0.3, 0.5, and 0.7) samples also possess a lamellar structure. Figure 2a shows a typical SEM image of the fractured surface of the $BaMn_{1.5}Zn_{0.5}Sb_2$ sample. The compositions of the samples were analyzed by EDS and their EDS spectra are similar. Figure 2b shows a typical EDS spectrum recorded on the fracture surface shown in Fig. 2(a), which reveals that the sample contains Ba, Mn, Zn and Sb. Quantitative EDS analysis results are given in Table 1. In Table 1, the Sb sites are assumed to be fully occupied (i.e., the Sb content is assumed to be 2 per unit formula). Although the

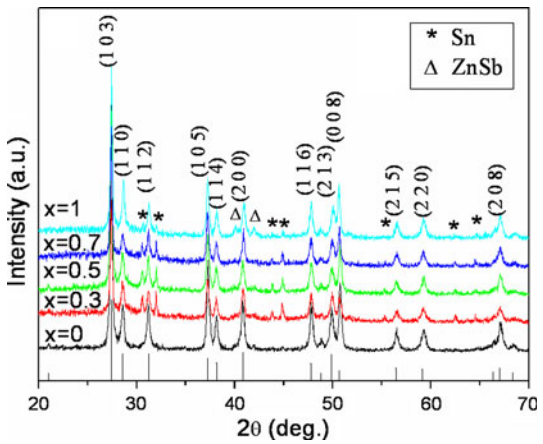

Fig. 1 Powder XRD patterns for the crystals synthesized using nominal compositions of $BaMn_{2-x}Zn_xSb_2$ (x = 0, 0.3, 0.5, 0.7, and 1) and reported data for $BaMn_2Sb_2$ (JCPDS card 33-0094) also given for comparison

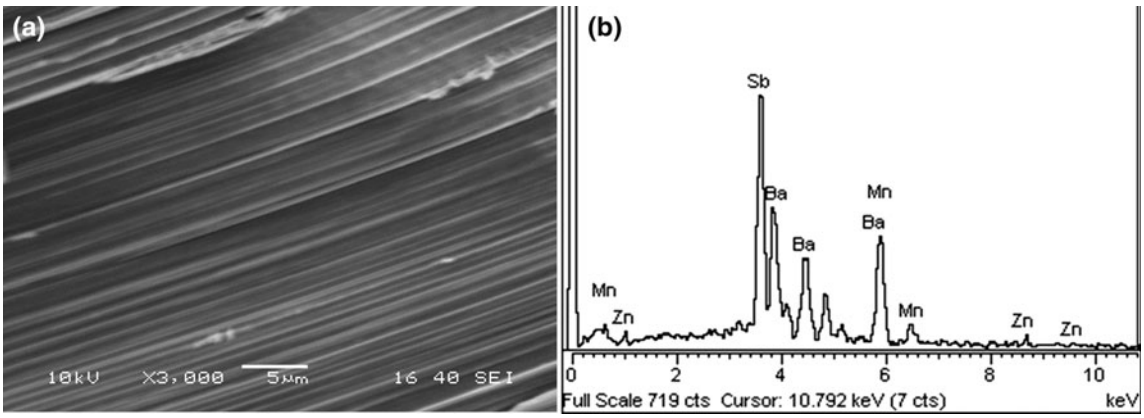

Fig. 2 Typical SEM image of the fracture surface of the $BaMn_{1.5}Zn_{0.5}Sb_2$ single crystal (**a**), and **b** EDS spectrum recorded on the fracture surface in (**a**)

Table 1 Quantitative EDS analysis results and some physical properties for the single crystals prepared using nominal compositions of $BaMn_{2-x}Zn_xSb_2$ (x = 0, 0.3, 0.5, 0.7)

Sample	EDS results	p (10^{16} cm^{-3})	μ (cm^2 V^{-1} s^{-1})	R_H (cm^3 C^{-1})
$BaMn_2Sb_2$	$Ba_{0.96}Mn_{1.87}Sb_2$	5.60	215	111.61
$BaMn_{1.7}Zn_{0.3}Sb_2$	$Ba_{0.94}Mn_{1.74}Zn_{0.14}Sb_2$	6.676	22.43	93.5
$BaMn_{1.5}Zn_{0.5}Sb_2$	$Ba_{0.97}Mn_{1.48}Zn_{0.35}Sb_2$	7.686	16.41	81.21
$BaMn_{1.3}Zn_{0.7}Sb_2$	$Ba_{0.99}Mn_{1.48}Zn_{0.56}Sb_2$	8.387	17.51	74.43

Zn content analyzed by EDS increases monotonically with the increasing of x value in the nominal composition, the actual Zn content for the samples is lower than the nominal Zn content x, which is probably due to evaporation of Zn during the synthesis processing.

Figure 3a shows the temperature dependence of electrical conductivity for the $BaMn_{2-x}Zn_xSb_2$ (x = 0, 0.3, 0.5, and 0.7) samples. As shown in Fig. 3a, the electrical conductivity of the $BaMn_{2-x}Zn_xSb_2$ samples monotonically increases with increasing temperature. At a given temperature, the electrical conductivity of the $BaMn_{2-x}Zn_xSb_2$ ($0 < x \leq 0.7$) samples is lower than that of the $BaMn_2Sb_2$ sample. This can be explained by the Hall effect measurement result (see Table 1) at room temperature. It is seen from Table 1 that the similar carrier mobilities of the Zn doped $BaMn_{2-x}Zn_xSb_2$ ($0 < x \leq 0.7$) samples are about one order of magnitude lower than the mobility of the $BaMn_2Sb_2$ sample (The significant reduction of carrier mobility of the Zn doped samples is most likely due to the strong scattering of carriers from the large lattice distortion around Mn sites partially substituted by Zn atoms), whereas the carrier concentration of the samples is not sensitive to the Zn content, and σ equals to $pq\mu$; therefore, the electrical conductivity of the $BaMn_2Sb_2$ decreases after Zn doping.

Figure 3b shows the temperature dependence of Seebeck coefficients for the samples studied. The Seebeck coefficients for all the samples are positive and decrease with increasing temperature. It can be seen from Fig. 3b that at a given temperature the Seebeck coefficients (also the electrical conductivity in Fig. 3a) do not change monotonically with the Zn content. This is because the actual compositions of the samples do not change monotonically with the Zn content. As indicated in Table 1, while the Zn and Ba contents increase with the nominal Zn content added, the Mn content for the samples of $BaMn_{1.5}Zn_{0.5}Sb_2$ and $BaMn_{1.3}Zn_{0.7}Sb_2$ remains the same. The Zn doped samples show much higher Seebeck coefficient than the $BaMn_2Sb_2$ at $T < 500$ K. The $BaMn_{2-x}Zn_xSb_2$ (x = 0.3) sample shows a maximum Seebeck coefficient value, 523 μV/K, at 300 K. In addition, the Seebeck coefficients of the Zn doped $BaMn_2Sb_2$ samples tend to be negative at high temperatures. For example, the Seebeck coefficient of the $BaMn_{1.5}Zn_{0.5}Sb_2$ sample changes from positive to negative at ~605 K, which reveals a compensated Seebeck coefficient due to competing n- and p-type carriers. At low temperatures, holes are the main carriers while at temperature above 605 K, electrons dominate. The similar character of compensated Seebeck coefficient is also found in $Yb_{11}Sb_{10}$ and $Ca_{11}Sb_{10}$ as reported in ref [22].

The power factors for the samples are calculated and shown in Fig. 3c. As shown in Fig. 3c, a maximum power factor value of ~0.063 μWcm^{-1} K^{-2} is obtained at 473 K for the $BaMn_{1.3}Zn_{0.7}Sb_2$ sample, which is ~3 times as large as that of the $BaMn_2Sb_2$ sample and the peak position for the power factor shifts to a higher temperature after Zn doping. The increase in power factor is due to the enhanced

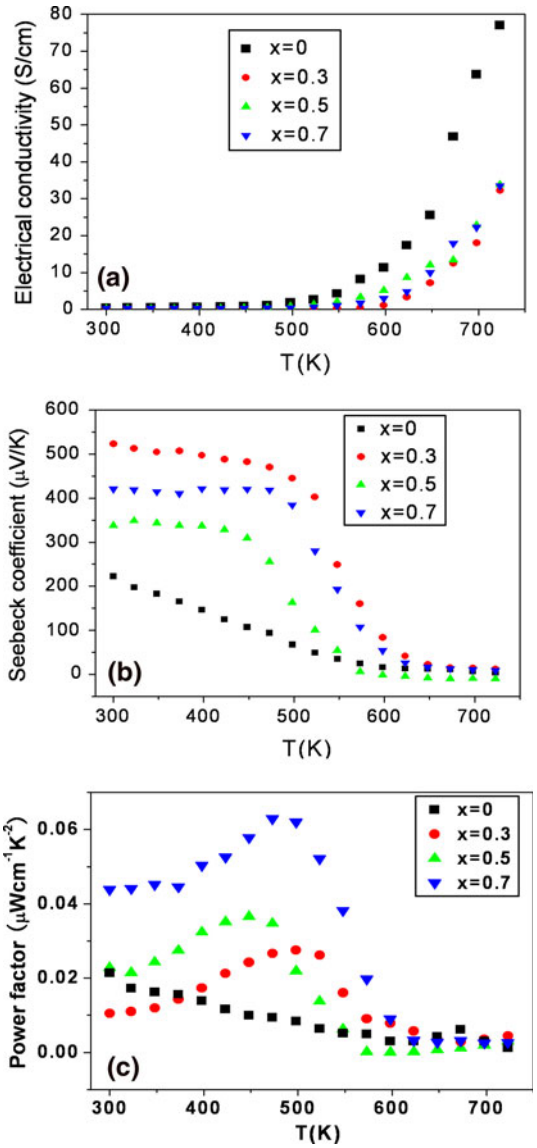

Fig. 3 Temperature dependence of electrical conductivity (**a**), **b** Seebeck coefficient, and **c** power factor for the single crystals prepared using nominal compositions of $BaMn_{2-x}Zn_xSb_2$ (x = 0, 0.3, 0.5, 0.7)

Seebeck coefficient. Moreover, power factor is close to zero at temperatures above 600 K, mostly due to the Seebeck coefficient close to zero.

4 Conclusions

$BaMn_{2-x}Zn_xSb_2$ (x = 0.3, 0.5, 0.7, and 1.0) crystals have been synthesized by the Sn-flux method. Less than half of the Mn in $BaMn_2Sb_2$ can be substituted by Zn under the present synthesis condition. The Seebeck coefficient can be significantly increased by Zn doping though with decreased electrical conductivity. The maximum power factor is about 0.063 $\mu Wcm^{-1} K^{-2}$ for $BaMn_{1.3}Zn_{0.7}Sb_2$ sample at 473 K, which is three times as high as that of the $BaMn_2Sb_2$ synthesized under the same condition.

Acknowledgments This work was supported by the National Natural Science Foundation of China (50872095). The authors thank Dr. Dehong Yu at Bragg Institute, ANSTO, Australia for polishing the manuscript.

References

1. L.E. Bell, Science **321**, 1457–1461 (2008)
2. D.M. Rowe (ed.), *CRC handbook of thermoelectrics* (CRC Press, USA, 1995)
3. G.J. Miller, in *Chemistry, structure and bonding of zintl phases and ions*, ed. by S.M. Kauzlarich (VCH, New York, 1996), p. 1
4. S.R. Brown, S.M. Kauzlarich, F. Gascoin, G.J. Snyder, Chem. Mater. **18**, 1873–1877 (2006)
5. J.F. Rauscher, S.M. Kauzlarich, T. Ikeda, G.J. Snyder, Z. Anorg. Allg. Chem. **633**, 1587–1594 (2007)
6. C. Candolfi, B. Lenoir, J. Leszczynski, A. Dauscher, E. Guilmeau, J. Appl. Phys. **105**, 083701 (2009)
7. L. Todorov, D.Y. Chung, L.H. Ye, A.J. Freeman, M.G. Kanatzidis, Inorg. Chem. **48**, 4768–4776 (2009)
8. A. Saramat, A.E.C. Palmqvist, A. Bentien, J. Alloys Compd. **477**, 51–54 (2009)
9. E.S. Toberer, S.R. Brown, T. Ikeda, S.M. Kauzlarich, G.J. Snyder, Appl. Phys. Lett. **93**, 062110 (2008)
10. S.R. Brown, E.S. Toberer, T. Ikeda, C.A. Cox, F. Gascoin, S.M. Kauzlarich, G.J. Snyder, Chem Mat **20**, 3412–3419 (2008)
11. E.S. Toberer, C.A. Cox, S.R. Brown, T. Ikeda, A.F. May, S.M. Kauzlarich, G.J. Snyder, Adv. Funct. Mater. **18**, 2795–2800 (2008)
12. A.F. May, E.S. Toberer, G.J. Snyder, J. Appl. Phys. **106**, 013706 (2009)
13. X.J. Wang, M.B. Tang, J.T. Zhao, H.H. Chen, X.X. Yang, Appl. Phys. Lett. **90**, 232107 (2007)
14. H. Zhang, J.T. Zhao, Y. Grin, X.J. Wang, M.B. Tang, Z.Y. Man, H.H. Chen, X.X. Yang, J. Chem. Phys. **129**, 164713 (2008)
15. X.J. Wang, M.B. Tang, H.H. Chen, X.X. Yang, J.T. Zhao, U. Burkhardt, Y. Grin, Appl. Phys. Lett. **94**, 092106 (2009)
16. H. Zhang, L. Fang, M.B. Tang, H.H. Chen, X.X. Yang, X.X. Guo, J.T. Zhao, Y. Grin, Intermetallics **18**, 193 (2010)
17. C. Yu, T.J. Zhu, S.N. Zhang, X.B. Zhao, J. He, Z. Su, T.M. Tritt, J. Appl. Phys. **104**, 013705 (2008)
18. E. Brechtel, G. Cordier, H. Schaefer, Z Naturforsch B **34B**, 921–925 (1979)
19. S.Q. Xia, C. Myers, S. Bobev, Eur. J. Inorg. Chem. **27**, 4262–4269 (2008)
20. J.M. An, A.S. Sefat, D.J. Singh, M.H. Du, Phys. Rev. B **79**, 075120 (2009)
21. H.F. Wang, K.F. Cai, H. Li, L. Wang, C.W. Zhou, J. Alloy. Compd. **477**, 519–522 (2009)
22. S.R. Brown, S.M. Kauzarich, F. Gascoin, G.J. Snyder, J. Solid State Chem. **180**, 1414–1420 (2007)